Chapter 4

Target Classification Using Adaptive Feature Extraction and Subspace Projection for Hyperspectral Imagery

Heesung Kwon, Sandor Z. Der, and Nasser M. Nasrabadi

U.S. Army Research Laboratory, ATTN: AMSRL-SE-SE, 2800 Powder Mill Road, Adelphi, MD 20783 {hkwon,sder,nnasraba}@arl.army.mil

Summary. Hyperspectral imaging sensors have been widely studied for automatic target recognition (ATR), mainly because a wealth of spectral information can be obtained through a large number of narrow contiguous spectral channels (often over a hundred). Targets are man-made objects (e.g., vehicles) whose constituent materials and internal structures are usually substantially different from natural objects (i.e., backgrounds). The basic premise of hyperspectral target classification is that the spectral signatures of target materials are measurably different than background materials, and most approaches further assume that each relevant material, characterized by its own distinctive spectral reflectance or emission, can be identified among a group of materials based on spectral analysis of the hyperspectral data.

We propose a two-class classification algorithm for hyperspectral images in which each pixel spectrum is labeled as either target or background. The algorithm is based on a mixed spectral model in which the reflectance spectrum of each pixel is assumed to be a linear mixture of constituent spectra from different material types (target and background materials). In order to address the spectral variability and diversity of the background spectra, we estimate a background subspace. The background spectral information spreads over various terrain types and is represented by the background subspace with substantially reduced dimensionality. Each pixel spectrum is then projected onto the orthogonal background subspace to remove the background spectral portion from the corresponding pixel spectrum.

The abundance of the remaining target portion within the pixel spectrum is estimated by matching a data-driven target spectral template with the background-removed spectrum. We use independent component analysis (ICA) to generate a target spectral template. ICA is used because it is well suited to capture the structure of the small targets in the hyperspectral images. For comparison purposes a mean spectral template is also generated by simply averaging the target sample spectra. Classification performance for both of the above-mentioned target extraction techniques are compared using a set of HYDICE hyperspectral images.

4.1 Introduction

Progress in automatic target recognition (ATR) techniques is crucial to the rapid development of digital battlefield technologies. Targets are generally man-made objects whose constituent materials and internal structures are substantially different from natural objects (i.e., backgrounds). The differences in materials and appearance between the targets and backgrounds lead to distinctive statistical and structural characteristics in images.

A large number of target classification/detection techniques have been developed based on broadband passive forward-looking infrared (FLIR) sensors that sense electromagnetic radiation in the 3–5 or 8–12 μm bands [1]. A commonly used multiple-band CFAR (constant false alarm rate) detection algorithm for a known signal pattern was introduced in [2]. An adaptive feature fusion technique has been recently developed, in which several local properties of the targets and backgrounds were jointly exploited within a local dual window and then fused to integrate different local features [3]. Statistical approaches have also been studied, in which the local statistical characteristics of the target and background regions were exploited by estimating, e.g., a probability density function [4], a co-occurrence matrix [5], or an eigen transformation matrix [6]. However, most previously attempted IR-based target detection techniques fail to produce satisfactory performance in the presence of high thermal clutter backgrounds or camouflaged targets.

Hyperspectral imaging sensors have been used in many remote sensing applications, such as reconnaissance, surveillance, environmental monitoring, and agriculture, because they capture more spectral information than a broadband IR sensor. Spectral information is obtained through a large number (often over a hundred) of narrow contiguous spectral channels, each channel capturing electro-magnetic reflectance or emission within the corresponding spectral range. The basic premise of hyperspectral target classification is that the spectral signatures of target materials are measurably different than background materials, and most approaches further assume that each relevant material, characterized by its own distinctive spectral reflectance or emission signature, can be identified among a group of materials. Anomaly detectors assume only the first, while spectral matching algorithms assume the latter as well.

We describe a two-class classification algorithm in which each pixel is labeled either target or background. The hyperspectral images we use were generated with the HYDICE (HYperspectral Digital Imagery Collection Experiment) sensor whose spectral range spans from 0.4 to 2.5 μm. In this spectral range the signal energy is dominated by reflected solar radiation rather than photon emission. The operation of the HYDICE sensor is normally limited to the daytime and the sensor cannot distinguish between hot and cold targets. Targets in our HYDICE images are combat platforms whose spectral characteristics depend largely on paint put onto a surface of the target.

Based on the linear spectral mixing models discussed in [7], the algorithm assumes that a reflectance spectrum of each pixel is a linear mixture of constituent spectra from disparate material types present in the pixel area. If a pixel spectrum includes a target spectrum, the pixel is labeled a target pixel. The pixel is classified as the background, if the target spectral contribution within the pixel spectrum is zero. Consequently, decomposition of the pixel spectrum into the constituent spectra is required in order to determine whether the target spectrum is present within the corresponding pixel spectrum. In order to successfully unmix the pixel spectrum, the spectral characteristics of the constituent materials have to be known a priori or be obtained from the data. In the proposed algorithm we obtain spectral information of the material types directly from the data.

The reflectance spectra in a spatial neighborhood, even from pixels within the same class of materials, are not identical mainly because of material variations and different illumination conditions. In addition, the background spectra generally consist of the combined reflectance spectra from a number of different natural objects, such as trees, grass, water, soil, etc. In order to address the spectral variability and diversity of the background spectra, a background subspace model is used to integrate key spectral signatures that spread over the background areas, into a subspace with substantially reduced dimensionality. Principal component analysis (PCA) is used to reduce the dimensionality of the original background space [8, 9, 10]; a relatively small number of significant eigenvectors are used to generate the background subspace.

In the proposed algorithm a target spectral template is created based on sample spectra. The target spectral template is then matched with the target spectral portion of the input pixel spectrum. Two methods are used to generate the target spectral template. A target spectral template generated by averaging the target sample spectra will not closely represent the true spectral characteristics of the target. Instead, we use independent component analysis (ICA) [11, 12, 13] to generate the target spectral template. ICA is applied to a portion of the HYDICE training images containing a small number of targets. The associated basis vector of the independent component showing the highest target prominence, is considered to represent the spectral feature of the target.

The target spectral portion within each pixel spectrum is obtained by removing the background spectral portion from the pixel spectrum. The removal of the background is performed by projecting the pixel spectrum onto the orthogonal background subspace. The orthogonal subspace projection for the subpixel target classification was first introduced by Harsanyi and Chang [14]. The amount of target spectrum within each pixel spectrum is then estimated by measuring the correlation between the target spectral portion and the target spectral template obtained from the ICA method.

This chapter is organized as follows. The HYDICE imaging system is briefly introduced in Section 4.2. A linear spectral mixing model for sub-

pixel target classification is described in Section 4.3. In Section 4.4 we present a brief introduction to ICA and ICA-based feature extraction for the hyperspectral data. In Section 4.5 an adaptive target classification algorithm based on orthogonal subspace projection is presented. Localized subspace estimation for the background is also introduced in Section 4.5. Two-class target classification results for the HYDICE images using the proposed algorithm are presented in Section 4.6. Conclusions are summarized in Section 4.7.

4.2 Hyperspectral Imaging System

Hyperspectral sensors operate in a variety of spectral bands, such as the visible, short-wave IR (SWIR: 1–2.5 μm), mid-wave IR (MWIR:3–5 μm), and long-wave IR (LWIR: 8–12 μm). The spectral range of the HYDICE sensors spans the visible and short-wave IR wavelengths where reflected solar radiation rather than object emission is the predominant source of energy. In the HYDICE imaging system, a group of spatially registered images, called a hyperspectral cube, is taken by an imaging spectrometer at a spectral range of 0.4 to 2.5 μm with a step size of 10 nm. The imaging spectrometer splits the reflected light (e.g., reflected sunlight and skylight) into narrow contiguous spectral channels, each channel generating an associated band image, as shown in Figure 4.1. Two-hundred-ten images are generated over the whole spectral range. For every pixel in the cube a spectral curve is then formed, which represents the spectral characteristics of the corresponding pixel, as shown in Figure 4.2.

4.3 Spectral Mixing Model

Airborne or tower-based hyperspectral imaging sensors normally view large areas on the ground, so the spatial resolution of the sensors is coarse in many applications. The area covered by each pixel in the hyperspectral images includes several constituent materials rather than a single material type. Consequently, a pixel spectrum is a mixture of the spectral signatures of the different constituent materials present. The detection (or classification) problem that deals with a mixed-pixel (subpixel) model has been intensively researched [7, 14, 15, 16]. We propose a target classification algorithm based on the spectral mixing model that estimates the abundances of the constituent spectra via spectral unmixing and matching to find whether the spectrum of the material of interest is present.

Our algorithm focuses on a two-class classification problem in which the pixel spectrum is considered a linear combination of individual spectra of two different material types — the target and background. In order to effectively address the spectral variability of the background spectra, we estimate a low-dimensional background subspace. The subspace is spanned by linearly

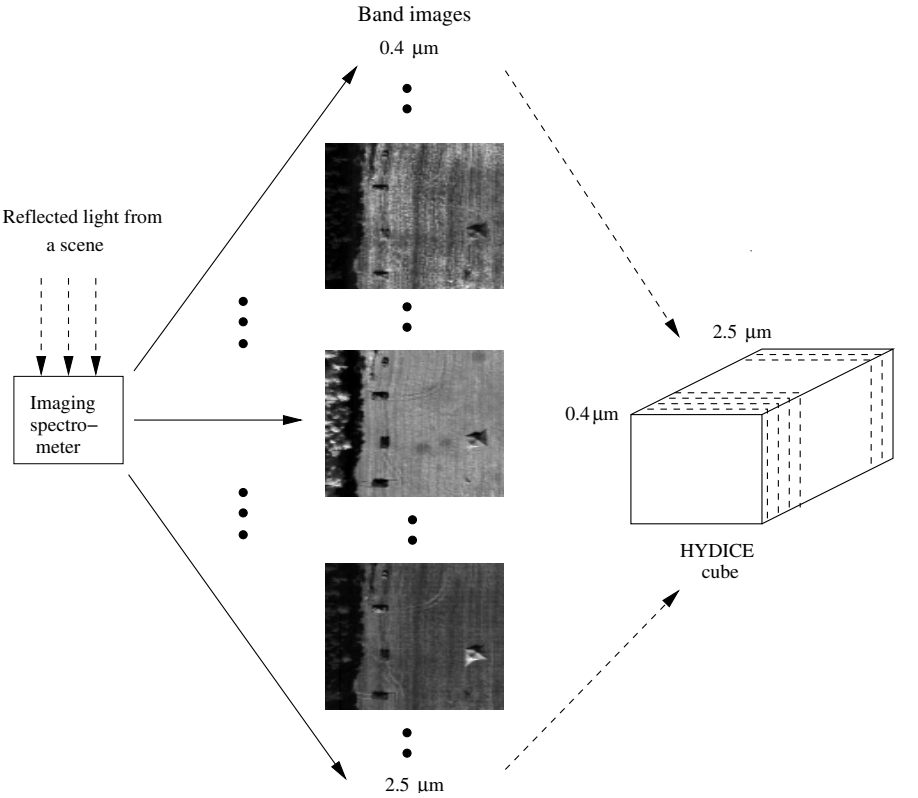

Figure 4.1. Hyperspectral imaging system

independent vectors $\mathbf{b}_1, \mathbf{b}_2, \ldots, \mathbf{b}_K$, which are the first K eigenvectors of a background covariance matrix; K is equal to the intrinsic dimensionality of the original background space.

The target spectrum varies, due mainly to the material variations and different illumination conditions. However, a single target spectral feature vector $\mathbf{s}_t$, an $M \times 1$ column vector, may still be capable of representing the target spectral characteristics in the data; M is the number of the spectral bands. Based on [17], the pixel spectrum $\mathbf{x}$, an $M \times 1$ column vector, is given by

$$\mathbf{x} = \begin{cases} \mathbf{s}_t a + \mathbf{B}\mathbf{c} + \mathbf{n}, & \text{if } 0 < a < 1, \\ \mathbf{B}\mathbf{c} + \mathbf{n}, & \text{if } a = 0, \end{cases} \tag{4.1}$$

where a is a scalar for target abundance, $\mathbf{B} = [\mathbf{b}_1 \mathbf{b}_2 \cdots \mathbf{b}_K]$ is an $M \times K$ matrix, $\mathbf{c} = (c_1, c_2, \ldots, c_K)^T$, $0 \leq c_1, c_2, \ldots, c_K < 1$, is a K-dimensional column vector whose components are the coefficients that account for the abundances of the corresponding endmember spectra $\mathbf{b}_1, \mathbf{b}_2, \ldots, \mathbf{b}_K$, and $\mathbf{n}$ is an M-dimensional column vector, representing Gaussian random noise. If $\mathbf{x}$ is

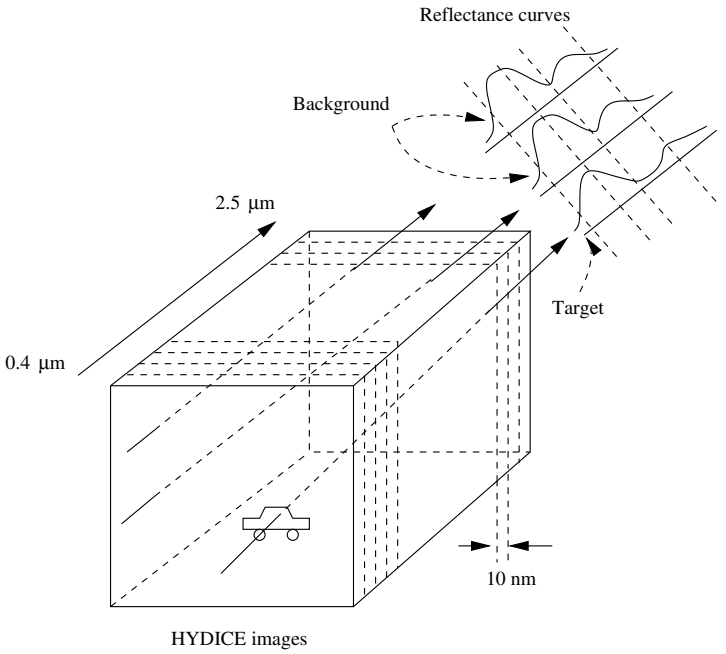

Figure 4.2. Creation of spectral reflectance curves from a hyperspectral cube.

the pixel spectrum from the target regions, the target abundance a is a non-zero value. On the other hand, a is zero if $\mathbf{x}$ is from the background region; in this case, $\mathbf{x}$ is a mixture of the background spectra only, as described in Equation (4.1). An accurate decision for the presence of the target spectrum within the pixel spectrum, therefore, can lead to successful classification of the individual pixel spectra.

The target feature vector $\mathbf{s}_t$ can be obtained from a spectral library or spectral samples in the given hyperspectral data. In the proposed algorithm the target feature is created from the sample spectra via an ICA-based feature extraction technique introduced in Section 4.4.

4.4 ICA-Based Feature Extraction

ICA, a relatively new concept in data representation, exploits high-order statistical dependencies among the data [11, 12, 13]. In this section, we introduce the ICA mixing and unmixing models and an ICA-based feature extraction technique. The feature extraction technique is based on the well-known ICA unmixing process [12], designed to find a feature vector that can closely represent the target spectral characteristics of the given data.

4.4.1 Independent Component Analysis (ICA)

Data representation in signal processing generally entails efficient removal of correlations present in the data. Principal component analysis (PCA) [8] is a well-known data transform technique that decorrelates the input data by exploiting pairwise second-order dependencies (e.g., covariance) and produces linearly independent variables, called principal components (or eigenvectors). Because the eigenvectors are only linearly independent from one another, nonlinear (high-order) statistical dependencies of the input data — as can be easily observed from sparse structures in an image, such as edges and small areas with relatively high contrast — cannot be removed [18]. ICA is a generalization of PCA where the input data is expressed as a linear mixture of statistically independent components which are nonlinearly decorrelated [11]. The independent components are, therefore, highly nongaussian (e.g., the Laplace distribution) and well suited to represent the sparse structures of the input data. We use ICA to better capture targets scattered in HYDICE images, each target occupying a small number of pixels. Detailed information on ICA and its applications for signal and image processing can be found in [19, 11, 12, 13, 20, 21, 18].

Suppose we are given the data X, consisting of M input images; the number of pixels in each image is N. Then X can be represented by an $M \times N$ matrix $[\mathbf{x}_1 \mathbf{x}_2 \cdots \mathbf{x}_N]$, each row, a N-dimensional vector, representing the corresponding input image. Each column $\mathbf{x}_i = (x_1, x_2, \ldots, x_M)^T$ is an M-dimensional vector whose components are the pixel values of the M images at the corresponding pixel location i. We denote by $S = [\mathbf{s}_1, \mathbf{s}_2, \ldots, \mathbf{s}_M]^T$ an $M \times N$ matrix, each row ${\mathbf{s}_i}^T$, an N-dimensional vector, representing the corresponding independent component image. The ICA mixing model is then defined by

$$X = AS, \tag{4.2}$$

where $A = [\mathbf{a}_1, \mathbf{a}_2, \ldots, \mathbf{a}_M]^T$ represents the $M \times M$ mixing matrix, each row ${\mathbf{a}_i}^T$, an M-dimensional basis vector, representing mixing coefficients that account for the abundances of the independent components for the ith input image. Equation (4.2) indicates that any given input image can be expressed as a linear combination of the independent component images whose abundances are specified in the corresponding row of A. Figure 4.3 shows a simplified schematic diagram of the ICA mixing and unmixing processes. In order to calculate A, we first estimate the unmixing matrix W of X using the basic assumption of ICA — the statistical independence of the components. Let the unmixing matrix $W = [\mathbf{w}_1, \mathbf{w}_2, \ldots, \mathbf{w}_M]^T$ be the inverse of the mixing matrix A. Equation (4.2) can then be expressed as

$$WX = S. \tag{4.3}$$

Figure 4.4 illustrates how matrix multiplications in Equation (4.3) are performed to unmix X. The unmixing process is basically a linear projection

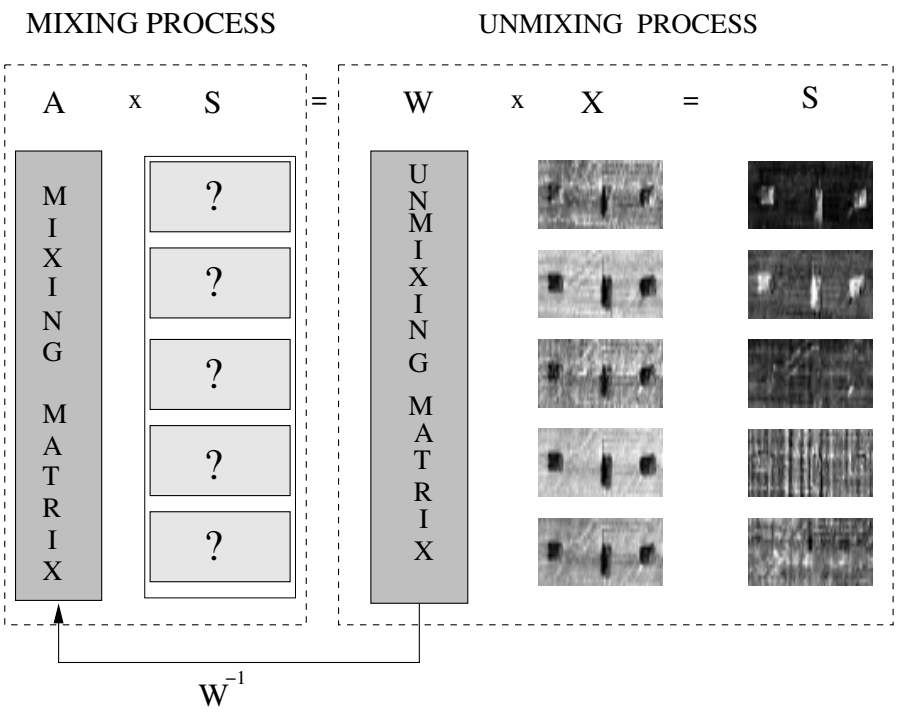

Figure 4.3. Simplified schematic diagram for the ICA mixing and unmixing processes

of X onto ${\mathbf{w}_i}^T$, $i = 1, 2, \ldots, M$, which are the basis vectors (axes) in a new coordinate system represented by Equation (4.3). ${\mathbf{w}_i}^T$ are actually the orthogonal basis vectors, and the input images are realigned along ${\mathbf{w}_i}^T$ to create the corresponding ICA component images. The independent components should be nongaussian, otherwise ICA cannot be achieved [11]. Accordingly, the directions of ${\mathbf{w}_i}^T$ are set such that nongaussianity of the ith independent component $\mathbf{s}_i = {\mathbf{w}_i}^T X$ is maximized.

4.4.2 ICA-Based Target Feature Extraction

Sample reflectance spectra collected from the pixels in the target regions (the targets in the scene are assumed to be the same kind) can be used directly to estimate the target spectral signature, e.g., by averaging them. However, in practice the material variations and different illumination conditions result in a broad range of spectral variability, as shown in Figure 4.5. Therefore, the individual spectra from the target regions, even from the same region, could be different. In this context the arithmetic mean of the sample reflectance spectra is not an adequate representation of the target spectral signature. We use an ICA-based feature extraction technique that focuses especially on extracting

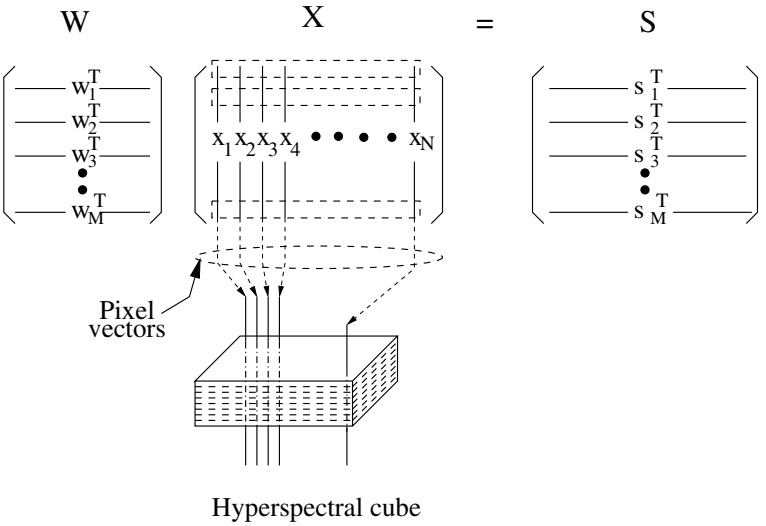

Figure 4.4. Matrix multiplications for the ICA unmixing process.

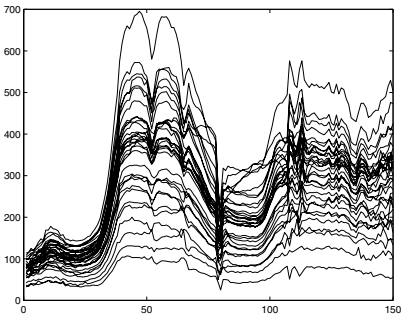

Figure 4.5. Example of spectral variability of the target reflectance spectra.

the independent components that form the target. In this technique a small hyperspectral cube is used to generate the target spectral feature vector.

Suppose we are given a relatively small hyperspectral cube $X = [\mathbf{x}_1 \mathbf{x}_2 \cdots \mathbf{x}_N]$, an $M \times N$ matrix, including the targets and the neighboring backgrounds. Normally, before unmixing X two preprocessing steps need to be taken — dimensionality reduction and whitening. Both the steps are based on the eigenvalue–eigenvector factorization described in [11]. The number of independent sources present in the data is closely associated with the intrinsic dimensionality L of the input data. L can be successfully determined by finding an optimum subspace of the input data, which is equivalent to a problem of finding a number of eigenvectors to be retained. Important studies have been performed to determine L based on probabilistic PCA models [9, 22]. We use the maximum likelihood PCA model introduced by Bishop [9] to cal-

culate L. L is normally far smaller than M; the input vectors in X are the column vectors $\mathbf{x}_i = (x_1, x_2, \ldots, x_M)^T$, $i = 1, 2, \ldots, N$. L has to be known a priori to decide how many independent components need to be created in the unmixing process.

The dimensionality reduction of X is normally accomplished by projecting X onto the first L eigenvectors of the covariance matrix of X. Whitening is a process in which the input data are uncorrelated and their variances become unity. Both the dimensionality reduction and whitening are performed by

$$X_s = U^{-1/2} E^T X, \tag{4.4}$$

where $X_s = [\mathbf{x}_1^s \mathbf{x}_2^s \cdots \mathbf{x}_N^s]$, an $L \times N$ matrix, is the transformed input data in the L-dimensional space, E is an $L \times M$ matrix, representing the first L eigenvectors, and U is a diagonal matrix whose main diagonal elements are the eigenvalues of E. The corresponding independent components $S_s = [\mathbf{s}_1^s, \mathbf{s}_2^s, \ldots, \mathbf{s}_L^s]$ can be obtained by

$$W_s X_s = S_s, \tag{4.5}$$

where $W_s = [\mathbf{w}_1^s \mathbf{w}_2^s \cdots \mathbf{w}_L^s]$ is the unmixing matrix in the L-dimensional space. Figure 4.6 illustrates the dimensionality reduction of the sample hyperspectral cube and the associated ICA unmixing process.

Each independent component image represents a set of corresponding projection values $\mathbf{s}_i = {\mathbf{w}_i}^T X$. The distributions of $\mathbf{s}_i$ are close to the Laplace distribution which has more pixels in tails and less pixels around the mean than the Gaussian distribution. Therefore, edges and small areas with high contrast are better represented by the independent component images. The structural details of the small targets in the sample hyperspectral cube are detected during the unmixing process, generating one or more ICA component images with greater target prominence (See the ICA component inside the rectangular box in Figure 4.6). The target prominence is measured by calculating the difference between the two values — the averages of the background pixels and target pixels in the ICA component image. As shown in Figure 4.6, the component images with higher target prominence include highly suppressed background where the mean and variation in pixel values are generally low. Once the component image with the highest target prominence $\mathbf{s}^{s*}$ is found, the corresponding ${\mathbf{w}^{s*}}^T$, the unmixing vector onto which X_s is projected to create $\mathbf{s}^{s*}$, is identified. The associated dewhitened vector of $\mathbf{w}^{s*}$ is then obtained by

$$\mathbf{g}^* = E U^{1/2} \mathbf{w}^{s*}. \tag{4.6}$$

$\mathbf{g}_i$, $i = 1, 2, \ldots, L$, are the column vectors of the mixing matrix A ($\mathbf{g}_i$ are shown in Figure 4.6). Each component of the M-dimensional vector $\mathbf{g}^*$ accounts for the abundance of $\mathbf{s}^{s*}$ in the associated band image. Therefore, $\mathbf{g}^*$ naturally represents the spectral characteristics of the target relative to those of the background in the given data. If the background spectral characteristics in

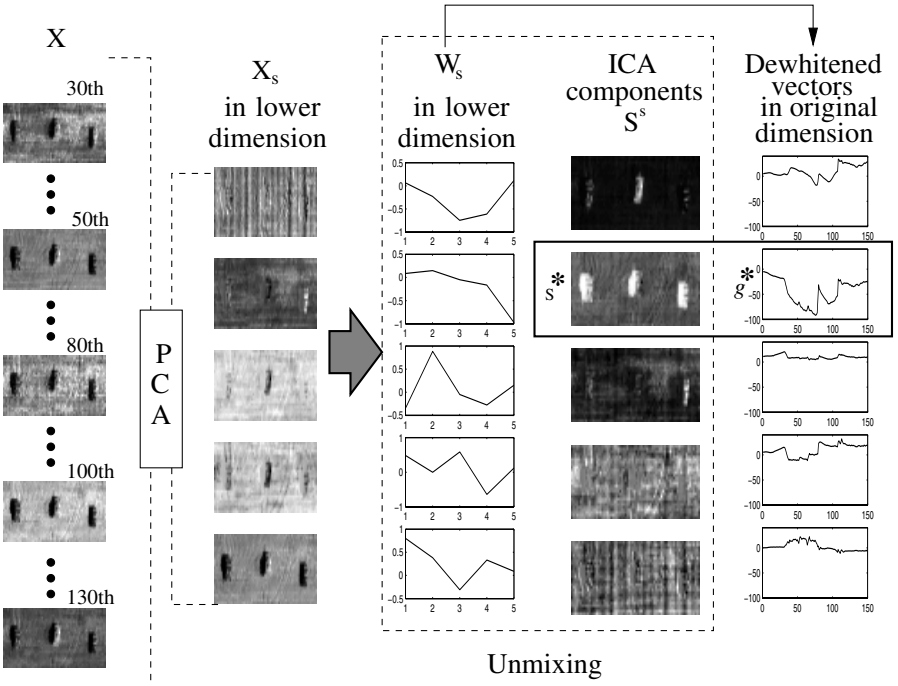

Figure 4.6. Schematic diagram of ICA-based feature extraction via the ICA unmixing process.

test images are not substantially different from those of the training images, we can apply $\mathbf{g}^*$ as a spectral template to the test images. If the targets are frequently situated among different background types, e.g., grass and soil, we generate multiple spectral templates, each template being adapted to the corresponding background type.

4.5 Subspace-Based Adaptive Target Classification

In this section, we estimate a low-dimensional subspace to address the background spectral variability. The subspace is spanned by a small number of linearly independent vectors (eigenvectors) directly estimated from the background spectra. Each pixel spectrum is projected onto the orthogonal background subspace to remove the spectral contribution due to the background materials. The target abundance of the pixel spectrum is then estimated by adaptive template matching.

4.5.1 Background Subspace Model

Suppose $\mathbf{x} = (x_1, x_2, \ldots, x_M)^T$ is an M-dimensional vector, representing a background reflectance spectrum. We denote by $C_{\mathbf{x}}$ the covariance matrix of the vector population of $\mathbf{x}$. M is equal to the number of spectral bands. We estimate the low-dimensional subspace $\langle \mathbf{B} \rangle$ spanned by first K eigenvectors $\mathbf{B} = [\mathbf{b}_1, \mathbf{b}_2, \ldots, \mathbf{b}_K]$ of $C_{\mathbf{x}}$; K is equal to the dimension of the subspace ($K \ll M$), and is set such that $\mathbf{B}$ accounts for most of the energy of the original background space. The construction of $\langle \mathbf{B} \rangle$ ensures that the most of the spectral information from the input space is integrated into the compact subspace with greatly reduced dimensionality.

4.5.2 Orthogonal Subspace Projection and Adaptive Spectral Matching

Orthogonal subspace projection is a geometrical approach originally devised to determine the least squares approximations to inconsistent linear algebraic equations (or linear systems) [23]. It has also been used for hyperspectral target classification/detection applications [14, 16]. Because the pixel spectrum is assumed to be a linear mixture of the target and the background constituent spectra, and $\langle \mathbf{B} \rangle$ is spanned by the key eigenvectors of the background covariance matrix, we can estimate the background portion $\mathbf{Bc}$ within the pixel spectrum $\mathbf{x}$ by projecting $\mathbf{x}$ onto the background subspace $\langle \mathbf{B} \rangle$, as shown Figure 4.7. The spectral contribution by the target and noise $\mathbf{w}$ is then estimated by simply subtracting the background contribution $\mathbf{P}_B\mathbf{x}$ from $\mathbf{x}$:

$$\mathbf{x} - \mathbf{P}_B\mathbf{x} = (I - \mathbf{P}_B)\mathbf{x}, \tag{4.7a}$$

$$= \mathbf{P}_B{}^{\perp}\mathbf{x}, \tag{4.7b}$$

where I is the identity matrix and $\mathbf{P}_B = \mathbf{B}(\mathbf{B}^T\mathbf{B})^{-1}\mathbf{B}^T$ is a background projection matrix, and $\mathbf{P}_B{}^{\perp}$ is an orthogonal projection matrix. For every pixel, adaptive template matching is performed to estimate the correlation between the target spectral contribution $\mathbf{P}_B{}^{\perp}\mathbf{x}$ within the pixel spectrum and the target spectral template $\mathbf{g}^{*T}$, which was obtained from Section 4.4.2:

$$F(\mathbf{x}) = \mathbf{g}^{*T}\mathbf{P}_B{}^{\perp}\mathbf{x}. \tag{4.8}$$

The pixels with higher values of $F(\mathbf{x})$ than a predefined threshold are then classified as the target.

4.5.3 Localized Background Subspace

The background subspace is estimated based on the sample spectra collected from various terrain types in the hyperspectral training images. Successful subspace modeling ensures robust and enhanced classification performance.

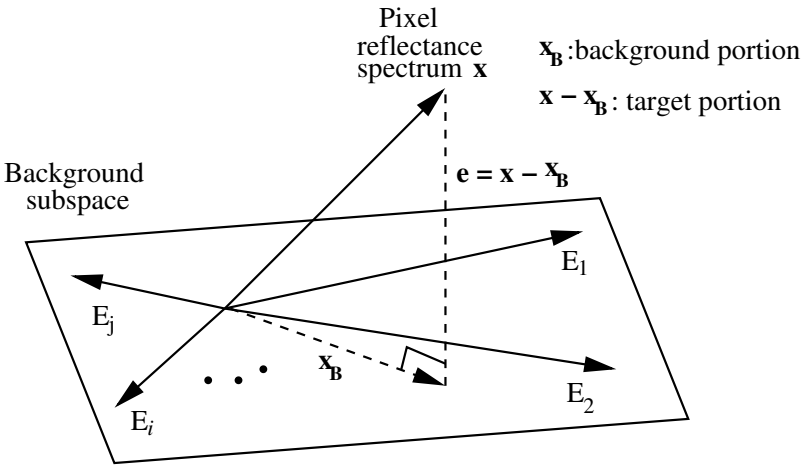

Figure 4.7. Orthogonal background projection.

Collecting the background spectra from the training images is normally performed by a human operator. Figure 4.8 shows the various background regions from which the sample spectra were collected. However, human intervention in a target classification process often results in inconsistent performance. It can be eliminated by replacing it with an automated procedure, in which the background subspace is estimated using the sample spectra directly collected from the hyperspectral sensor. In this section we introduce an unsupervised segmentation technique developed by the authors [24] to estimate the background subspace adapted to the local characteristics of the hyperspectral test images. In the technique the reflectance spectra in the test images are first segmented into two classes based on spectral dissimilarity.

The spectral dissimilarity is measured within a local window. A relatively large fixed-size local window is placed around each pixel. Note that each pixel corresponds to a pixel vector (spectrum) in the spectral domain. The spectral dissimilarity d_i associated with pixel location i is defined as

$$d_i = \frac{\sum_{j \in \mathcal{B}} \|\mathbf{s}_j - \mathbf{s}_i\|}{N_i}, \tag{4.9}$$

where $\|\cdot\|$ represents the Euclidean norm, $\mathcal{B}$ represents a set of pixels selected randomly from within the local window, as shown in Figure 4.9. The vectors $\mathbf{s}_i$ and $\mathbf{s}_j$ represent the corresponding pixels at locations i and j, respectively, and N_i represents the number of the selected pixels (the randomly selected pixels and neighboring pixels) required to estimate d_i. After the spectral dissimilarity of every pixel is obtained, a spectral dissimilarity image D is formed, as shown in Figure 4.10. Each element of the image represents the amount of the average spectral difference between the center pixel and its randomly selected neighbors. The spectral dissimilarity image provides a set of spectral-

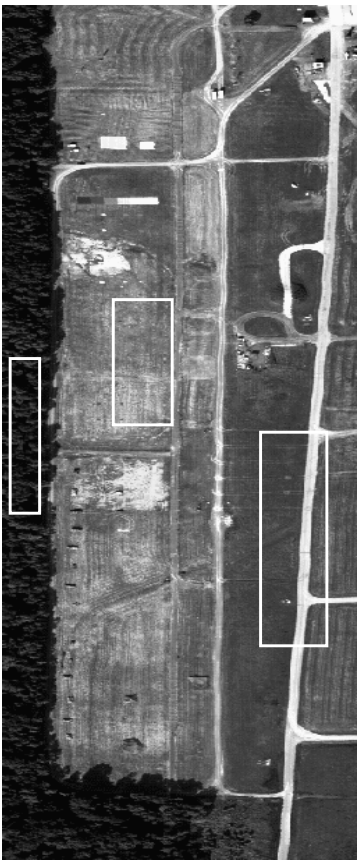

Figure 4.8. Sample background spectra from the hyperspectral images to estimate the sample-based background subspace; the samples were collected from the rectangular regions.

feature values d_i suitable for clustering. The pixels in the targets regions tend to have greater values than those of the background pixels, because of the spectral difference between the two material types. The pixels associated with smaller d_i are then identified as the background whose spectra are used to estimate the background subspace. Segmentation is performed by applying a simple thresholding method to the feature values in D whose statistics are closely associated with the contents of the HYDICE images — mainly the complexity of the backgrounds. The threshold is calculated by averaging the mean and the maximum value of D.

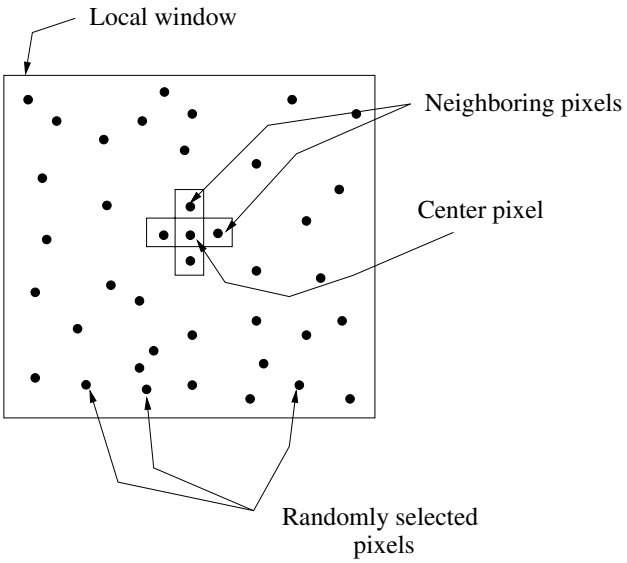

Figure 4.9. Randomly selected pixels and neighboring pixels within the local window for calculation of spectral dissimilarity.

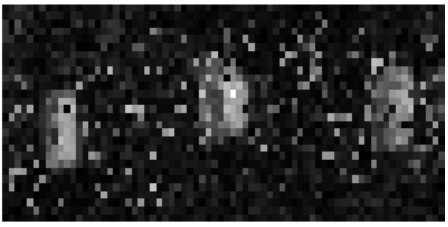

Figure 4.10. Spectral dissimilarity image D of the small hyperspectral cube.

4.6 Experimental Results

In this section we apply the proposed ICA-based adaptive matching technique to the HYDICE images to detect targets of interest. The HYDICE imaging sensor generates 210 band images across the whole spectral range (0.4–2.5 μm), each band covering a narrow spectral range of 10 nm. We, however, use only 150 band images by discarding water absorption and low signal-to-noise ratio (SNR) bands; the band images used are the 23rd–101st, 109th–136th, and 152nd–194th. The low SNR bands were identified by human observation of sample spectra. The test cubes were provided with the associated ground truth maps. The coordinates of the centers of the targets in the ground truth map were compared with those of the detected targets to check if the classification was accurate.

4.6.1 Target Feature Extraction

Figures 4.11–4.13 show typical reflectance curves from the regions of the disparate material types, such as targets, trees, and grass. Even though a distinguishable spectral pattern can be found among a group of reflectance curves of the same material type, a wide range of spectral variability, prevailing in all the material types, hinders correct and accurate classification of the targets from the surrounding backgrounds. In particular, the reflectance curves from the target region, as shown in Figure 4.11, display substantial intraclass variability, showing how seriously material variations and different illumination conditions interfere with the hyperspectral target classification process.

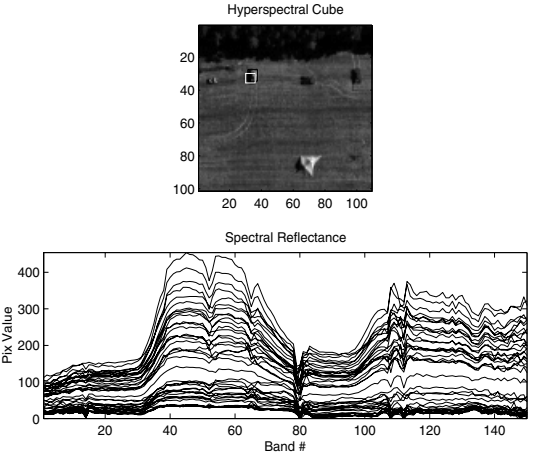

Figure 4.11. Spectral variability in the target region.

In order to estimate the target abundance within the individual pixel spectra, we generate a spectral feature vector, used as a correlation template in the classification process, to represent the target spectral characteristics in the given data. Two methods are used to create the spectral feature vector — mean curve generation and ICA-based feature extraction. We compare the target classification performance associated with the two feature generation methods. Figure 4.14 shows the sample target spectral reflectance curves and the corresponding mean spectral curve $\mathbf{m}_t^T$. The ICA-based spectral feature extraction technique, based on [20], uses a set of training images $X = [\mathbf{x}_1 \mathbf{x}_2 \cdots \mathbf{x}_N]$ which are usually a small-sized hyperspectral cube with the single background type, as shown in Figure 4.6. The intrinsic dimensionality L of the input vectors $\mathbf{x}_i$ (the pixel spectrum vector) was obtained based on the maximum likelihood PCA model [9]; L was 5 instead of 150, meaning that the column vector $\mathbf{x}_i^s$, $i = 1, 2 \ldots, N$, are in the 5-dimensional space, and there exists not more than five independent sources in the training im-

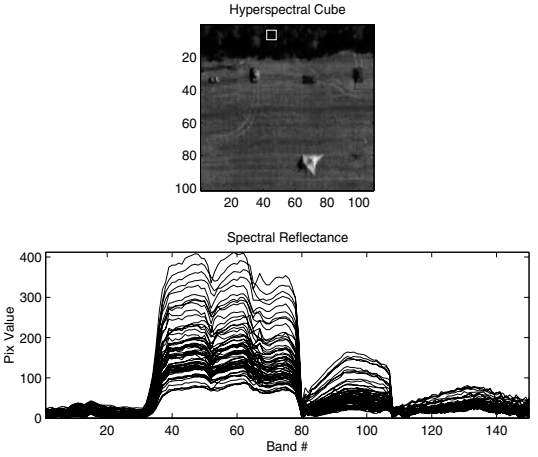

Figure 4.12. Spectral variability in the tree region.

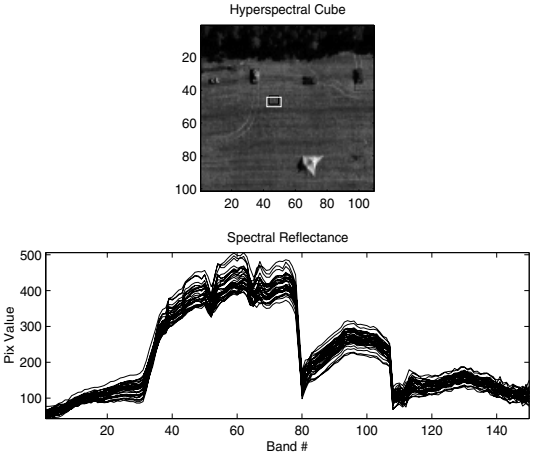

Figure 4.13. Spectral variability in the grass region.

ages. Figure 4.6 shows the training images X and a schematic diagram of the ICA unmixing process, in which the training images are decomposed into the five ICA component images. In the unmixing process the first five principal component images X_s were actually used to calculate the corresponding ICA component images. The direction of each of the five unmixing vectors $\mathbf{w}_i^{sT}$, $i = 1, 2, \ldots, 5$, was set such that nongaussianity of the corresponding ICA component $\mathbf{s}_i^s$ was maximized. The 150-dimensional vectors $\mathbf{g}_i$ were then obtained by first dewhitening $\mathbf{w}_i^s$ and then projecting them back to the original measurement space. The ICA component image with the highest target prominence $\mathbf{s}^{s*}$ and its associated basis vector $\mathbf{g}^{*T}$ are shown in Figure 4.15.

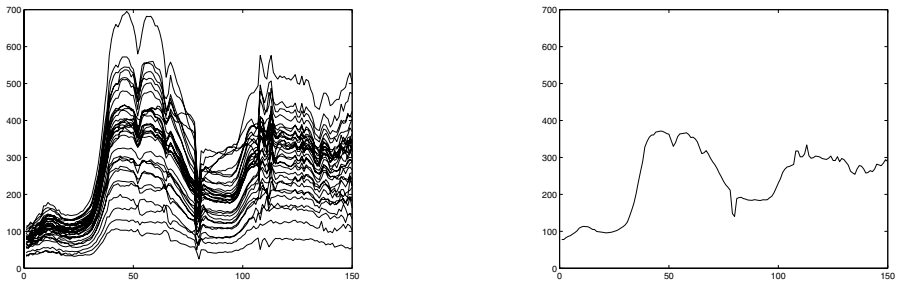

Figure 4.14. (a) Sample target reflectance curves and (b) the corresponding mean curve $\mathbf{m}_t^T$.

$\mathbf{g}^{*T}$ is used as a target spectral template in the target classification process

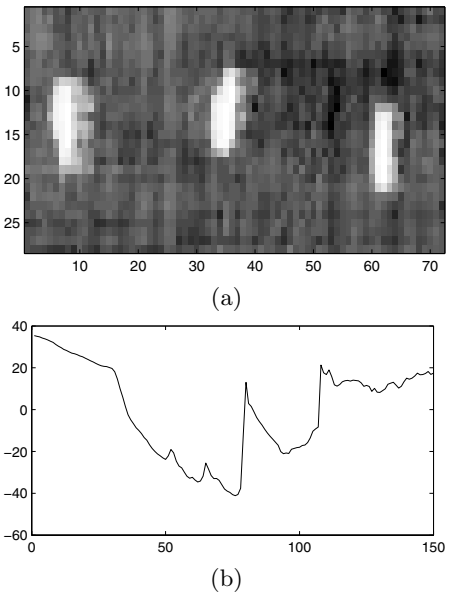

Figure 4.15. (a) ICA component image with the highest target prominence and (b) its corresponding basis vector $\mathbf{g}*^T$.

to measure the significance of the target contributions within the individual background-removed pixel spectra. The spectral shape of $\mathbf{g}^{*T}$ is quite different from that of $\mathbf{m}_t^T$. This is because the direction of $\mathbf{g}^{*T}$ is set such that it suppresses the background spectra, while emphasizing the target spectra. $\mathbf{m}_t^T$, in contrast, is generated only to detect the target spectra, regardless of the spectral characteristics of the backgrounds of the given hyperspectral data.

4.6.2 Background Subspace Estimation

Figure 4.16 shows two hyperspectral band images, each from either of the two hyperspectral cubes, Cube I and II, to be used as test images for target classification. Cube I includes five targets (four vehicles and one man-made

(a) (b)

Figure 4.16. Sample band images from two hyperspectral test cubes, (a) Cube I and (b) Cube II.

object) and two different types of background (trees and grass). Cube II is smaller than Cube I in size and includes three targets (all of them are vehicles) and the single background type of grass.

We first estimate the background subspace to remove the background portion from every pixel spectrum in the test cubes. Two different techniques were used to estimate the background subspace: localized subspace estimation and sample-based subspace estimation. In order to estimate the localized subspace $\langle \mathbf{B}_l \rangle$, we first apply the unsupervised segmentation, described in Section 4.5.3, to the corresponding hyperspectral test cube. For each test cube, $\langle \mathbf{B}_l \rangle$ is spanned by the first eight eigenvectors of the covariance matrix of the pixel spectra in the regions classified as the background.

Figure 4.17 shows the spectral dissimilarity matrices and unsupervised segmentation results for the two test cubes. The size of the local sliding window was half the size of the test image. We used 80 randomly selected pixels and four neighboring pixels of the corresponding input pixel in the local window to estimate the spectral dissimilarity. A simple threshold-based technique was used to segment the dissimilarity matrices. The segmentation of Cube II was successful since most of the background areas were segmented out of the image. Cube I includes more diverse backgrounds than Cube II. In the segmentation of Cube I the area covered by grass was successfully classified as background, while most of the tree regions were not. This is mainly because of the irregular spectral reflectivity of the tree regions. Accordingly, for Cube I most of the background spectra used to estimate the localized subspace were collected from the grass areas.

The sample-based background subspace $\langle \mathbf{B}_s \rangle$ was estimated for both the test cubes based on the sample spectra collected from various types of the

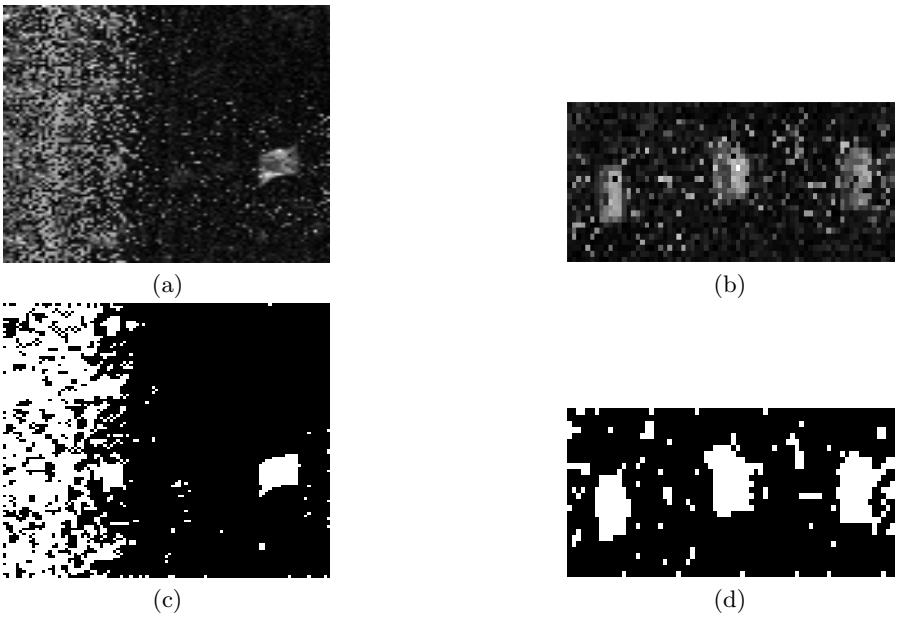

Figure 4.17. Spectral dissimilarity images for (a) Cube I and (b) Cube II and the corresponding segmentation results for (c) Cube I and (d) Cube II.

backgrounds in the hyperspectral training images (inside the rectangular boxes), as shown in Figure 4.8; the same number of eigenvectors used to estimate $\langle \mathbf{B}_l \rangle$ was used to estimate $\langle \mathbf{B}_s \rangle$. It should be noted that modeling of $\langle \mathbf{B}_s \rangle$ involves a human operation, incurring inconsistent classification performance.

Once $\langle \mathbf{B}_l \rangle$ and $\langle \mathbf{B}_s \rangle$ are estimated, the associated orthogonal projection matrixes ${\mathbf{P}_{B_l}}^{\perp}$ and ${\mathbf{P}_{B_s}}^{\perp}$, respectively, are readily calculated. Figure 4.18 shows three band images from Cube I and their corresponding background-removed images, in which the background portion of every pixel spectrum is discarded by projecting the pixel spectrum $\mathbf{x}$ onto ${\mathbf{P}_{B_l}}^{\perp}$ and ${\mathbf{P}_{B_s}}^{\perp}$. The background removal was quite successful for both the subspace estimation methods. The localized subspace estimation is preferable for the given test cubes because it provides comparable performance to that of the sample-based method and allows automated target classification. However, as HYDICE images include increasingly complex backgrounds (e.g., urban areas), the dissimilarity measure for the localized subspace estimation fails to work properly because of a high level of the spectral dissimilarity inside the background. In general, the choice between the sample-based and the localized subspace estimations needs to be made in the context of background complexity. Therefore, it is necessary to further develop an appropriate measure of the background complexity for hyperspectral imagery as future work.

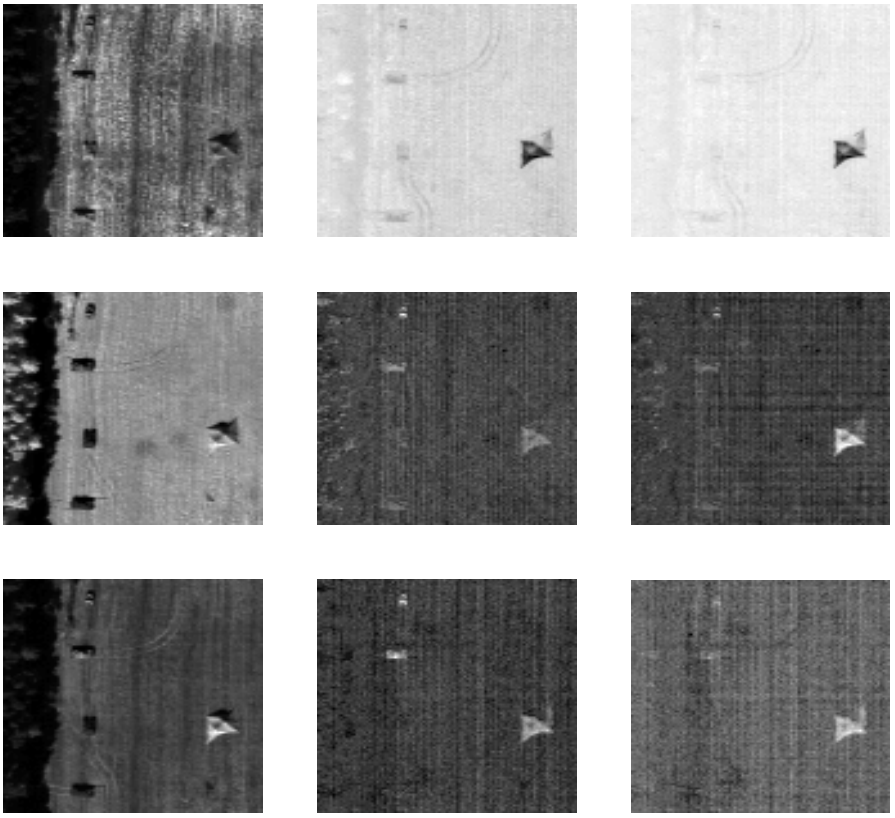

Figure 4.18. Example of the background-removed images based on the localized and sample-based subspace estimation. The images in the first column are the three band images from Cube I. The images in the second and third column are the corresponding background-removed band images based on $\mathbf{P}_{B_l}{}^{\perp}\mathbf{x}$ and $\mathbf{P}_{B_s}{}^{\perp}\mathbf{x}$, respectively.

4.6.3 Adaptive Target Classification

After removing the background portion from every pixel in the hyperspectral test cube, we estimate the target abundance within the pixel spectrum by calculating $\mathbf{m}_t^T\mathbf{P}_B{}^{\perp}\mathbf{x}$ and $\mathbf{g}^{*T}\mathbf{P}_B{}^{\perp}\mathbf{x}$; $\mathbf{m}_t^T$ and $\mathbf{g}^{*T}$ serve as the target spectral templates. Quantitative performance of the proposed algorithm, such as the receiver operating characteristic (ROC) curves, was not evaluated mainly because of a lack of HYDICE images. Figure 4.19 shows the target abundance images and the corresponding classification results for Cube I and Cube II using the mean-based spectral template $\mathbf{m}_t^T$, which is shown in Figure 4.14. The sample-based background subspace $\langle \mathbf{B}_s \rangle$ was used in the mean-based target classification. Because the mean curve cannot inherently address a wide range of spectral variability of the target, only partial targets were detected for both

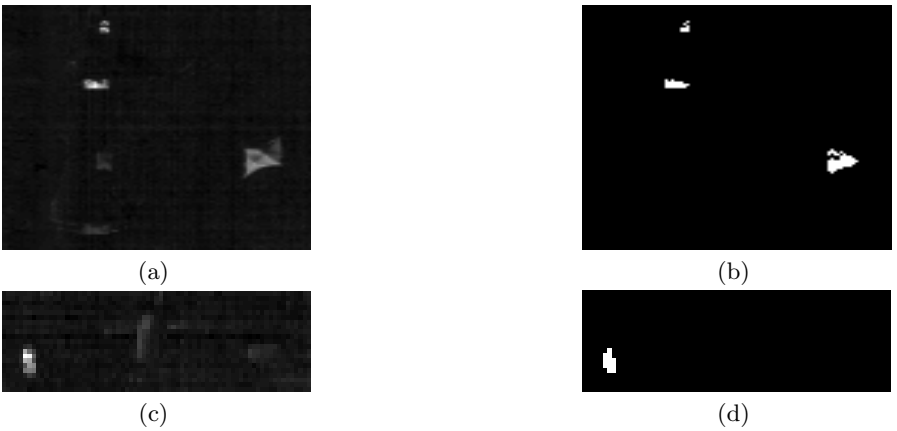

Figure 4.19. Target classification based on the mean-based spectral template and the sample-based subspace estimation. (a) Target abundance image and (b) classification results for Cube I. (c) Target abundance image and (d) classification results for Cube II.

the test cubes. Figures. 4.20 and 4.21 show the target abundance images and the corresponding classification results using the ICA-based spectral template $\mathbf{g}^{*T}$ for both the sample-based and the localized background subspace models, respectively. A complete set of the targets was successfully detected for both the subspace models, demonstrating the superiority of the ICA-based classification over the mean-based technique.

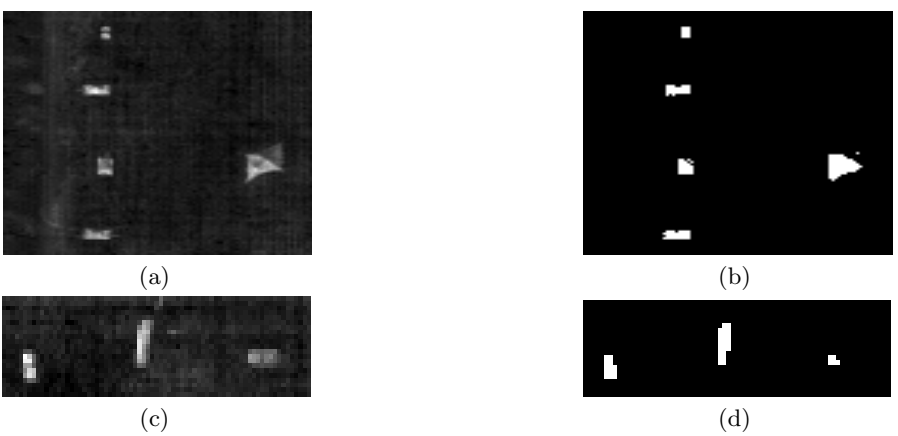

Figure 4.20. Target classification results based on the ICA-based spectral template and the sample-based subspace estimation. (a) Target abundance image and (b) classification results for Cube I. (c) Target abundance image and (d) classification results for Cube II.

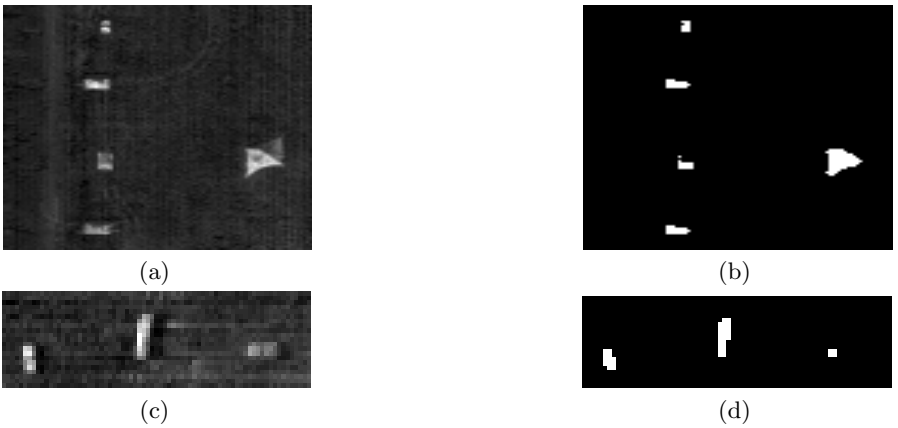

Figure 4.21. Target classification results based on the ICA-based spectral template and the localized subspace estimation. (a) Target abundance image and (b) classification results for Cube I. (c) Target abundance image and (d) classification results for Cube II.

The ICA-based target classification without background removal from the individual spectra was also applied to the test cubes by calculating ${\mathbf{g}^*}^T\mathbf{x}$. The experiments were performed to find how significantly the background removal process contributed to the target classification process. The projection ${\mathbf{g}^*}^T\mathbf{x}$ was not able to suppress the background portion within the pixel spectra, drastically increasing the false classification in the background regions, as shown in Figure 4.22.

4.7 Conclusions

We have presented a two-class target classification algorithm, in which an individual pixel spectrum is linearly decomposed into constituent spectra and then labeled either target or background. The background and target spectral characteristics are represented by the low-dimensional background subspace and the target feature vector generated by the ICA-based feature extraction, respectively.

The background subspace model has been used to address a wide range of spectral variability by integrating key spectral features of various terrain types into the low-dimensional subspace. In order to fully automate the target classification process, the localized background subspace model has been also developed, in which the eigenvectors spanning the subspace are calculated based on the reflectance spectra directly from the background regions of the test images. Unsupervised segmentation based on the spectral dissimilarity is applied to the test images to identify the potential background regions. In our

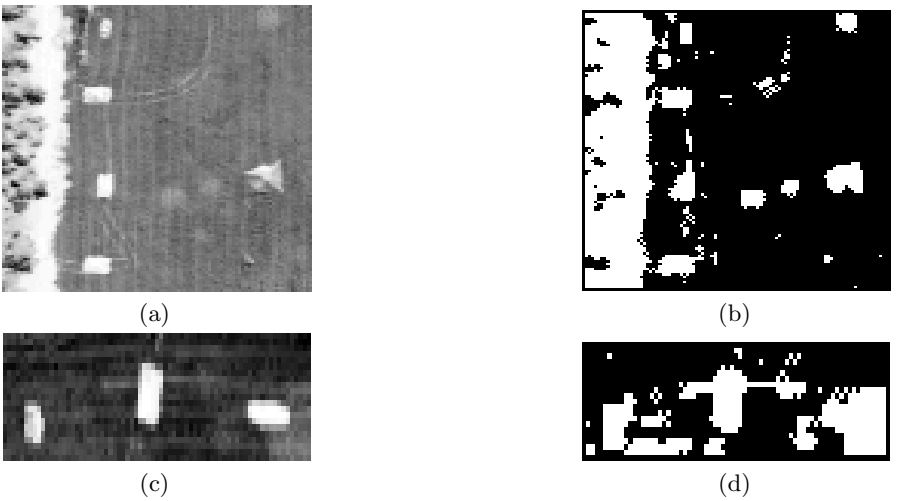

Figure 4.22. Target classification results without background removal. (a) Target abundance image and (b) classification results for Cube I. (c) Target abundance image and (d) classification results for Cube II.

experiments, the localized and sample-based subspace models in the proposed classification technique provides comparable classification performance.

The background portion is removed from each pixel spectrum by projecting it onto the orthogonal background subspace. The background removal process greatly improves target classification performance, as supported by the simulation results. The abundance of the remaining target spectral portion is estimated by measuring the correlation between the background-removed individual pixel and the target template to identify the intrinsic spectral nature of the corresponding pixel surface. The target features obtained by both the ICA-based and mean-based feature extraction techniques are used as the target spectral templates. The nonlinear data structures of the targets are exploited by the ICA-based feature extraction. Consequently, ICA-based feature extraction results in better classification performance than mean-based extraction.

Due to the lack of HYDICE images available for experiment, only the qualitative performance was evaluated. In order to further investigate the usefulness of the proposed algorithm, a quantitative performance measure such as the ROC curve needs to be calculated using a larger data set that includes blind test images.

The types of paint used for the targets in our data set is unknown (it may be the three-color camouflage paint). Analysis of the spectral characteristics of different types of paint on the surface of military targets is desirable and needs to be conducted as future work. It will help develop robust tar-

get detection/classification methods that can be used in various battlefield environments, e.g., wooded (and/or grassy) areas and barren desert.

4.8 Acknowledgment

This research was sponsored by the U.S. Army Research Laboratory (ARL) and was accomplished under the ARL/ASEE postdoctoral fellowship program, contract DAAL01-96-C-0038. The views and conclusions contained in this document are those of the authors and should not be interpreted as representing the official policies, either expressed or implied, of ARL or the U.S. government. The U.S. government is authorized to reproduce and distribute reprints for government purposes, notwithstanding any copyright notation herein.

References

[1] Bhanu, B.: Automatic target recognition: State-of-the-art survey. IEEE Transactions on Aerospace and Elect. Syst. **22** (1986) 364–379
[2] Reed, I.S., Yu, X.: Adaptive multiple-band CFAR detection of an optical pattern with unknown spectral distribution. IEEE Transactions Acoustics, Speech and Signal Process. **38** (1990) 1760–1770
[3] Kwon, H., Der, S.Z., Nasrabadi, N.M.: Adative multisensor target detection using feature-based fusion. Optical Engineering **41** (2002) 69–80
[4] Schachter, B.J.: A survey and evaluation of FLIR target detection/segmentation algorithm. In: Proc. of DARPA Image Understanding Workshop. (1982) 49–57
[5] Aviram, G., Rotman, S.R.: Evaluating human detection performance of targets and false alarms, using a statistical texture image metric. Optical Engineering **39** (2000) 2285–2295
[6] Chan, L., Nasrabadi, N.M., Torrieri, D.: Eigenspace transformation for automatic clutter rejection. Optical Engineering **40** (2001) 564–573
[7] Manolakis, D., Shaw, G., Keshava, N.: Comparative analysis of hyperspectral adaptive matched filter detector. In: Proc. SPIE. Volume 4049. (2000) 2–17
[8] Joliffe, I.T.: Principal Component Analysis. Springer-Verlag, New York (1986)
[9] Bishop, C.M.: Baysian PCA. In: Neural Information Processing System. Volume 11. (1998) 382–388
[10] Rajan, J.J., Rayner, P.: Model order selection for the singular value selection and the discrete Karhunen-Loeve transform using a bayesian approach. IEE Proc. Image Signal Process **144** (1997) 116–123
[11] Hyvärinen, A., Oja, E.: Independent component analysis: Algorithms and applications. Neural Networks **13** (2000) 411–430

[12] Hyvärinen, A.: Survey on independent component analysis. Neural Computing Surveys **2** (1999) 94–128
[13] Hyvärinen, A.: Sparse code shrinkage: Denoising of nongaussian data by maximun likelyhood estimation. Neural Computation **11** (1999) 1739–1768
[14] Harsanyi, J.C., Chang, C.I.: Hyperspectral image classification and dimensionality reduction: An orthogonal subspace projection approach. IEEE Transactions Geosci. Remote Sensing **32** (1994) 779–785
[15] Ashton, E.L.: Detection of subpixel anomalies in multispectral infrared imagery using an adaptive bayesian classifier. IEEE Transactions Image Process. **36** (1998) 506–517
[16] Chang, C.I., Zhao, X.L., Althouse, M., Pan, J.J.: Least squares subspace projection approach to mixed pixel classification for hyperspectral images. IEEE Transactions Geosci. Remote Sensing **36** (1998) 898–912
[17] Manolakis, D., Shaw, G.: Detection algorithms for hyperspectral imaging applications. IEEE Signal Processing Magazine **19** (2002) 29–43
[18] Bartlett, M.S.: a dissertation: Face Image Analysis by Unsupervised Learning and Redundancy Reduction. University of California, San Diego (1998)
[19] Comon, P.: Independent component analysis: A new concept? Signal Processing **36** (1997) 287–314
[20] Hyvärinen, A.: Fast and robust fixed-point algorithms for independent component analysis. IEEE Transactions Neural Networks. **10** (1999) 626–634
[21] Lee, T.W., Girolami, M., Sejnowski, T.J.: Independent component analysis using an extended infomax algorithm for mixed subgaussian and supergaussian sources. Neural Computation **11** (1999) 417–441
[22] Minka, T.P.: Automatic choice of dimensionality for PCA. M.I.T Media Laboratory Perceptual Computing Section Technical Report (2000)
[23] Strang, G.: Linear Algebra and Its Applications. Harcourt Brace & Company (1986)
[24] Kwon, H., Der, S.Z., Nasrabadi, N.M.: An adaptive unsupervised segmentation algorithm based on iterative spectral dissimilarity measure for hyperspectral imagery. In: Proc. SPIE. Volume 4310. (2001) 144–152